Design and Demonstration of an In-Plane Silicon-on-Insulator Optical MEMS Fabry–Pérot-Based Accelerometer Integrated With Channel Waveguides

Kazem Zandi, Joseph André Bélanger, and Yves-Alain Peter, *Senior Member, IEEE*

***Abstract*—In this paper, we present a novel optical microelectromechanical systems (MEMS) accelerometer sensor dedicated to space applications. An in-plane Fabry–Pérot (FP) microcavity (FPM) with two distributed Bragg reflectors (DBRs) is used to detect the acceleration. One of the DBR mirrors is attached to two suspended proof masses, allowing the FP gap to change while proof masses experience acceleration. Acceleration is then detected by measuring the spectral shift of the FPM. The optical accelerometer presented here uses silicon strip waveguides integrated with MEMS on a single silicon-on-insulator wafer, making it compact and robust. All of the device components are fabricated using one single fabrication step. Immunity to electromagnetic interference, high sensitivity and resolution capability, integrability, reliability, low cross-sensitivity, simple fabrication, and possibility of having two- and three-axis sensitivities are numerous advantages of our sensor compared to the conventional ones. The sensor performance demonstrated a 90-nm/g sensitivity and 111-μg resolution and better than 250-mg dynamic range. [2012-0098]**

***Index Terms*—Distributed Bragg reflector (DBR), Fabry–Pérot (FP), optical accelerometer, silicon-on-insulator (SOI), waveguides.**

I. Introduction

MICROELECTROMECHANICAL systems (MEMS) capacitance accelerometers are currently used in spacecraft navigation systems [1], but they suffer from low SNR (which limits their sensitivity), high power consumption, temperature dependence, and high cross-sensitivity and are not immune to electromagnetic interference [2], making them unsuitable for microsatellite applications.

Optical MEMS sensors are frequently used for industrial process, aerospace, and military application owing to their immunity to electromagnetic interference and possibility of operation in hazardous and high-temperature environments [3].

Manuscript received April 23, 2012; revised July 10, 2012; accepted July 13, 2012. Date of publication August 27, 2012; date of current version November 27, 2012. This work was supported in part by the Canadian Space Agency. An earlier version of this paper was presented at the 23rd lEEE Conference on Micro Electro Mechanical Systems, Hong Kong, China, January 24–28, 2010. Subject Editor S. Merlo.

The authors are with the Department of Engineering Physics, École Polytechnique de Montréal, Montréal, QC H3C 3A7, Canada (e-mail: kazem.zandi@polymtl.ca; joseph-andre.belanger@polymtl.ca; yves-alain.peter@polymtl.ca).

Color versions of one or more of the figures in this paper are available online at http://ieeexplore.ieee.org.

Digital Object Identifier 10.1109/JMEMS.2012.2211577

Optical accelerometers have been investigated previously. Most of them are based on variable optical attenuator [4]–[6], optical diffraction detection [7], [8], antiresonant reflecting optical waveguides [2], Fresnel diffractive microlens [9], photoelastic effect [10], or wavelength dependence [11]. Out-of-plane MOEMS accelerometers based on light reflectance spectrum variation were also reported where the reflectance spectrum of a photonic band gap structure changes as a function of external accelerations [12], [13]. Some of the reported accelerometers are based on the combination of optical fibers and micromachined silicon [4]–[6], [11], [14]. In some cases, they have low sensitivity due to the low reflectivity of the Fabry–Pérot (FP) mirrors [11], [14]. Although, in some cases, they can be very sensitive [6], [7], they are not fully integrated, and they have a limited reliability because of their misalignment sensitivity to vibration/shock. μg-resolution optical accelerometers based on FP were demonstrated, but they are out of plane, not integrated, large in size, and expensive to fabricate, making them inappropriate for microsatellite missions [15].

Over the last decade, small satellites and their application toward space science missions have increased. Their need for attitude control necessities have developed toward full three-axis stabilization and precise pointing knowledge and control. This is associated with the requirement for compact low-power accelerometers and gyroscopes. Therefore, achieving an integrated high-performance low-cost miniature sensor chip is desired to reduce the spacecraft operating costs and to improve the system performance for mission accomplishment and autonomous navigation.

Microphotonic integrated circuits are composed of two or more photonic devices on a single substrate. The main difficulty that microphotonics should solve is system integration. Integrating different optical components on a single substrate will reduce the amount of external fiber-optic interconnections, consequently decreasing the overall system mass and size, and also optimize the system reliability as well as cost efficiency.

Silicon photonics can bring together both conventional integrated optics using ridge waveguides of several micrometers in cross section and nanophotonics structures where silicon-on-insulator (SOI) is used as platform. Using the SOI platform has two advantages; first, it decreases the size of integrated optical structures due to the high refractive index contrast between silicon and air, and second, it is compatible with CMOS technology.

Here, we present a novel in-plane waveguide-integrated optical MEMS accelerometer fabricated on SOI wafer. Our device is based on an FP filter with distributed Bragg reflector (DBR) mirrors utilizing strip silicon waveguides. The device can be integrated with other optical functions since the structure is in plane, it is robust and reliable since only MEMS structures are used in the sensor part, it is sensitive since an FP interferometer with relatively high reflectivity mirrors are used as the sensor part, and it is a low-cost device since all the sensor components are fabricated in one simple fabrication step.

The aim of this work is to achieve a low-power, small-size, simple-fabrication, high-performance, and reliable navigation sensor for low-cost future small satellites/spacecrafts.

II. Principle of Operation

Fig. 1(a) shows the schematic of our proposed optical accelerometer. The device is based on an in-plane FP microcavity (FPM) with two DBR mirrors utilizing strip silicon waveguides, in which one DBR mirror is attached to two suspended proof masses. As a consequence of acceleration, the relative displacement of the movable mirror with respect to the fixed one changes the cavity length and modifies the FP resonance [Fig. 1(b) and (c)].

A. Principle of Optical Detection

The resonance wavelength peak λ of an FPM with air gap is directly related to the gap x by [Fig. 1(b)]

$$x = \frac{m\lambda}{2} \tag{1}$$

where m is the order of the resonance.

The static response of an accelerometer with a suspended mass of M (proof mass) and spring constant of k is defined by combining Newton's second law and Hook's law and is given by

$$a = -\frac{k}{M}\Delta x = -\omega_n^2 \Delta x \tag{2}$$

where a is the acceleration, ω_n is the natural frequency of the system in the sensing direction, and Δx is the relative displacement of the suspended mass (movable DBR mirror) with respect to the fixed parts of the structure [Fig. 1(b)].

The relationship equation between the FPM acceleration sensor output and its experienced acceleration is then given by combining (1) and (2)

$$a = -\frac{m\omega_n^2 \Delta\lambda}{2} \tag{3}$$

where $\Delta\lambda$ is the FPM spectral shift. It can be seen from this relationship that the sensitivity and resolution of the device are controlled by the optical $(\Delta\lambda)$ and mechanical (ω_n) characteristics.

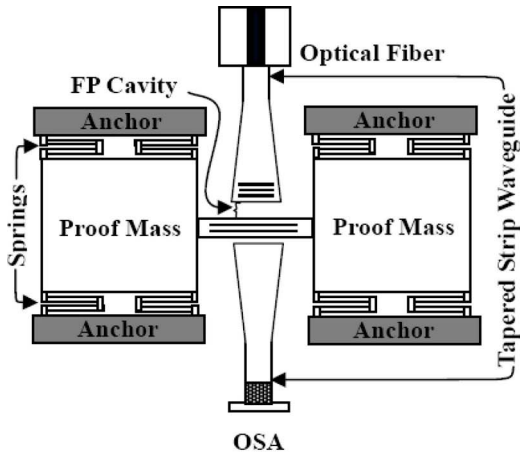

(a)

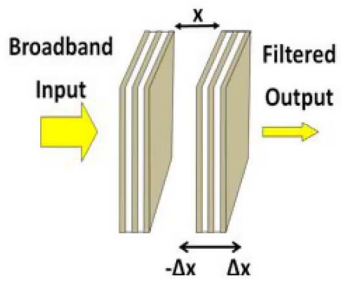

(b)

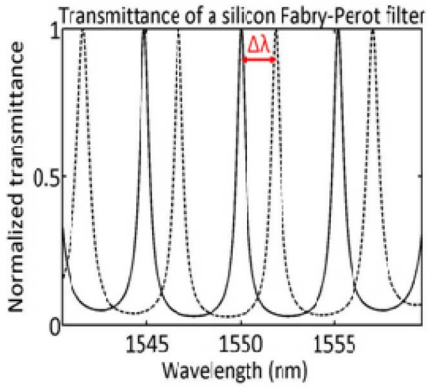

(c)

Fig. 1. (a) Schematic of the accelerometer based on FP filter. (b) Schematic of the FPM made of two DBR mirrors. (c) Transmission spectrum shift of the FPM due to the 48-nm displacement of one mirror.

B. Mechanical Sensor Model

The accelerometer is symmetrical and consists of two proof masses suspended by eight serpentine flexure beams [Fig. 1(a)]. Accelerations parallel to the wafer plane and perpendicular to the DBR mirrors cause the proof masses to move in the wafer plane. The static response of such a suspended mass in the y-direction is defined by (2)

$$a = -\frac{k_y}{M}\Delta y = -\omega_{ny}^2 \Delta y \tag{4}$$

where M is the proof mass, Δy is the proof mass displacement in the y-direction, k_y is the device spring stiffness in the y-direction, and ω_{ny} is the natural frequency of the system in the y-direction.

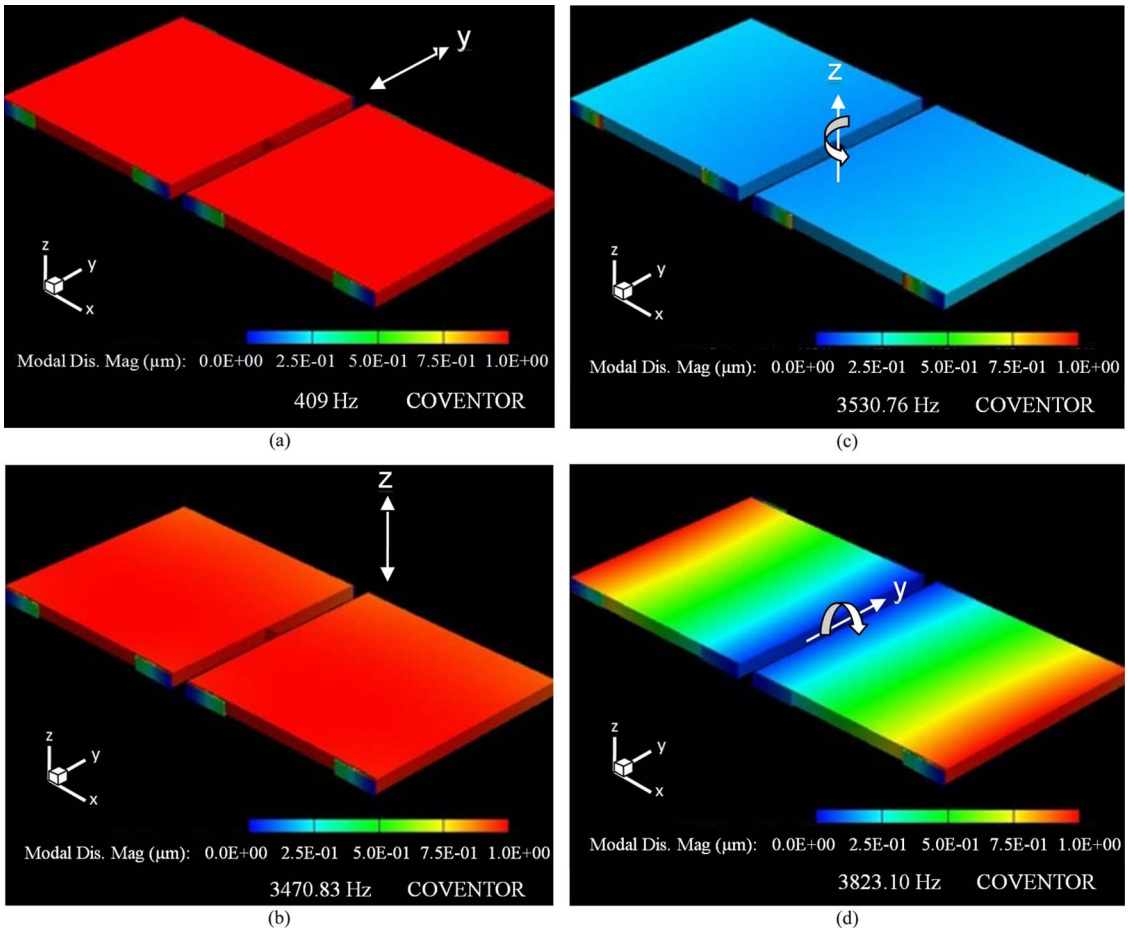

Fig. 2. Simulated first four modes of the device: (a) Normal mode (resonant at 409 Hz). (b) Second mode (resonant at 3.48 kHz). (c) Third mode or trunnion mode (resonant at 3.53 kHz). (d) Fourth mode (resonant at 3.82 kHz). The arrows in the pictures show the displacement (or rotation) for each mode.

Using basic beam theory, the spring constants of a fixed-end beam with length l, width w, and thickness t are given by

$$k_y = \frac{Etw^3}{l^3} \tag{5}$$

$$k_x = \frac{2Etw}{l} \tag{6}$$

$$k_z = \frac{Ewt^3}{l^3} \tag{7}$$

where E is Young's modulus ($\sim$160 GPa for silicon).

A serpentine flexure beam consists of two span beams and three connector beams. The considered dimensions for its components are as follows: span beam length: 470 μm, span beam width: 3 μm, and $connector\ beam\ width = connector\ beam\ length = 10\ \mu$m.

Since the width of the connector beams is much larger than the width of the span beams, we can consider a serpentine flexure beam as a serial of two fixed-end beams. The effective spring constant k_s of two springs that are connected in series is then given by

$$\frac{1}{k_s} = \frac{1}{k_1} + \frac{1}{k_2} = \frac{2}{k_i} \Rightarrow k_s = \frac{k_1}{2} = \frac{Etw^3}{2l^3} = 0.62\ \text{N/m} \tag{8}$$

where k_1 and k_2 are the spring constants of two fixed-end beams which are equal in this case. Since the device consists of eight serpentine springs in parallel, the total effective spring constant of the device is $k_{\text{tot}} = 8k_s = 4.8$ N/m.

The spring constant of the device was simulated by finite-element modeling using Coventorware 2010 and found to be $K = 6.125$ N/m. The difference between theory and simulation originates from the estimation we have made for the serpentine spring.

The main challenge in designing accelerometers is the manufacturing of a sensor which is sensitive to acceleration in the desired direction but insensitive to all other cross-axis directions. The cross-sensitivity of the device is investigated using mode analysis. Fig. 2 shows the first four possible modes of the structure. Owing to the optical characteristics, the sensor is insensitive to excitations that result in parallel motion of the Bragg mirrors (modes 2 and 4) since the length of the FPM remains unchanged. However, it is sensitive to the angular or trunnion deflection (mode 3) since the optical path of light in the FPM changes in this case [Fig. 3(b)]. Although, under the excitation of the resonant trunnion mode, no wavelength shift is generated, the transmitted power through the device at the resonant wavelength is modulated due to the finesse reduction of the microcavity caused from parallelism deviation [16]. Since the frequency of this mode is well above the sensor

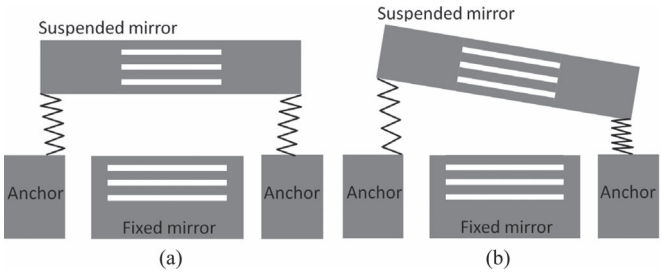

Fig. 3. Two expected sensitive modes for the sensor. (a) Normal mode. (b) Trunnion mode.

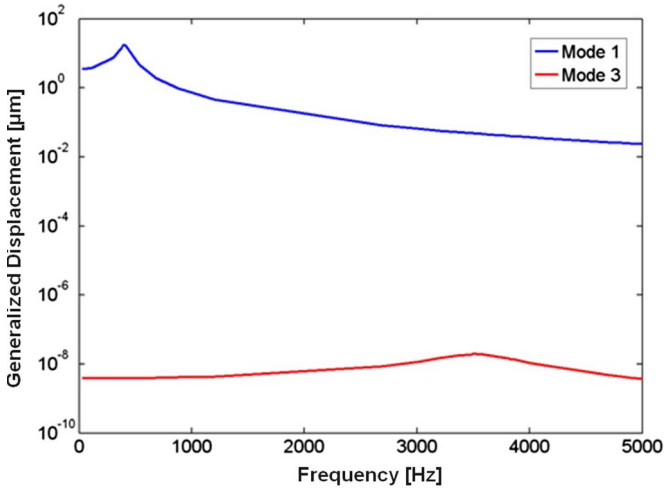

Fig. 4. Simulated frequency response of the system for the (Mode 1) normal and (Mode 3) trunnion modes.

working bandwidth, it can be suppressed over the sensing bandwidth.

Fig. 4 represents the simulated frequency response of the system for normal and trunnion modes.

III. Fabrication

The device fabrication process flowchart is shown in Fig. 5(a). The device is fabricated using one single deep reactive ion etching (DRIE) step on a 30-μm SOI wafer with 3-μm-thick buried oxide. A 30-μm-thick silicon device layer is used in order to have a larger proof mass leading to better sensitivity of the sensor. Suspension beams, proof masses, DBR mirrors, and strip waveguides are fabricated by DRIE. After wafer saw-cut dicing and polishing, which are critical processes for having waveguides with good-quality edges and facets, the remaining buried oxide is removed using vapor HF etching to release the structure and prevent the devices from sticking to the substrate. A mechanical method is used for the SOI strip waveguide polishing. Fig. 5(b) shows a 3-D atomic force microscopy (AFM) image of the surface profile of the waveguide facet after polishing.

The rms roughness of the facet surface is approximately 3.5 nm which is good enough when telecommunication wavelength range is used. Two proof masses $(8.1 \times 10^{-7}$ kg) are suspended on eight springs having a designed overall stiffness of 6.125 N/m providing a 438-Hz resonance frequency. The fabricated device is shown in Fig. 6. The FP cavity is formed

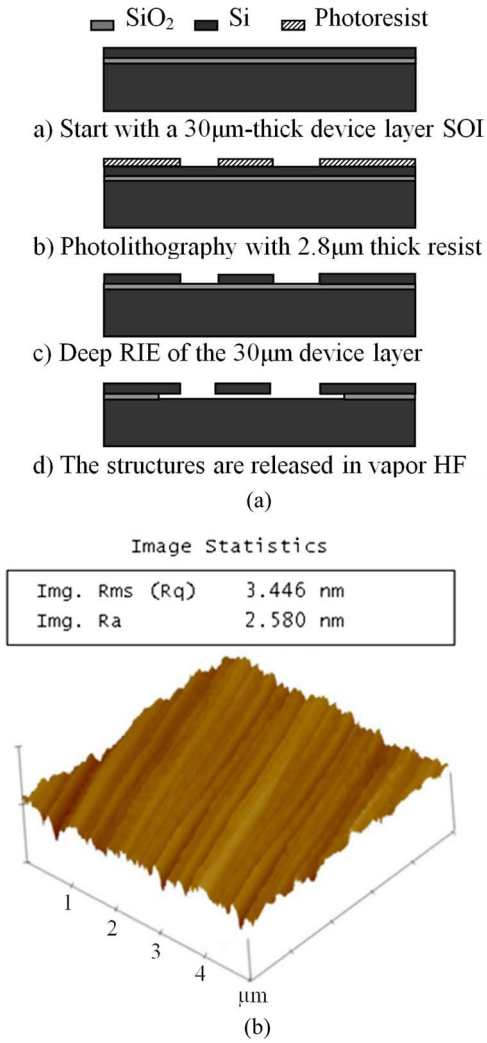

Fig. 5. (a) Microfabrication steps for the FP-based accelerometer. (b) Three-dimensional AFM image of the waveguide facet surface profile after polishing.

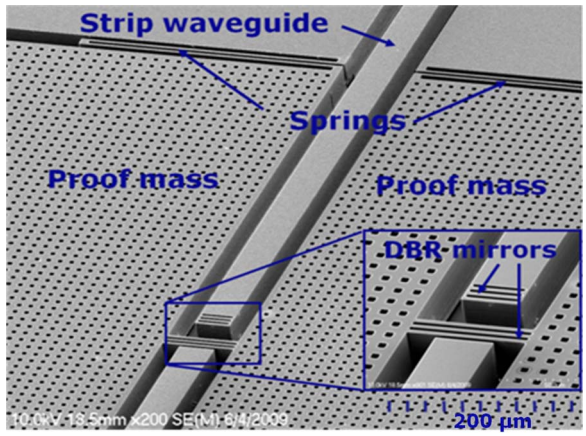

Fig. 6. SEM of the silicon-microfabricated FP-based accelerometer.

by two Bragg mirrors each made of three silicon walls (inset of Fig. 6). The thicknesses of the silicon walls and air layers for the Bragg mirrors are 3.1 and 2.4 μm, respectively. The movable DBR mirror is attached to the proof masses and is displaced when exposed to acceleration, producing a reduction in the length of the air gap of the FP filter. The other DBR

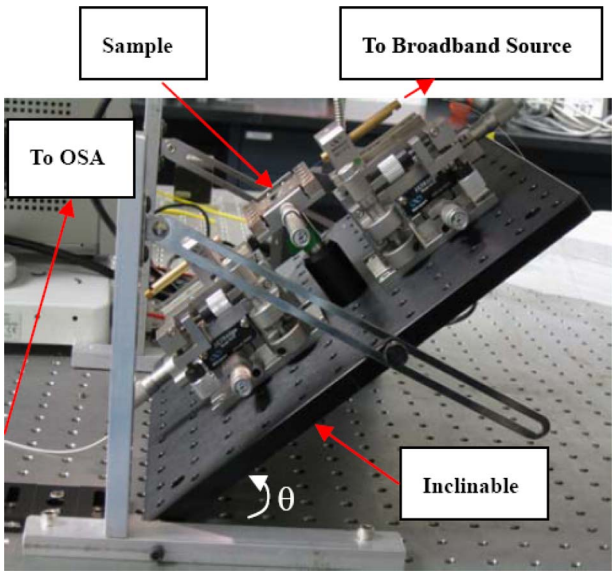

Fig. 7. Optical setup for the characterization of the accelerometer.

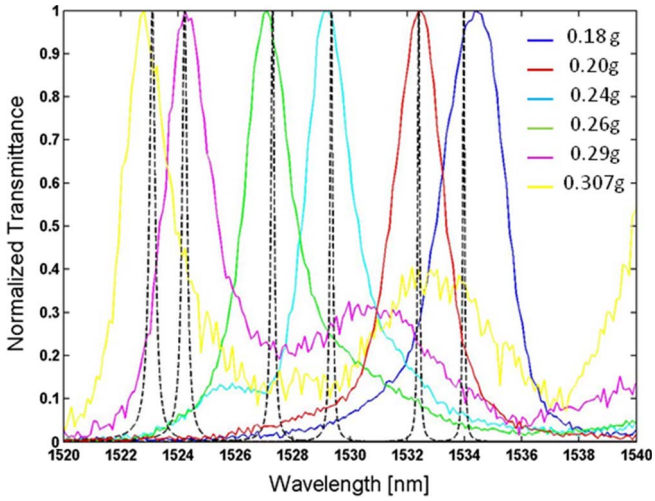

Fig. 8. (Colored curves) Measured and (black-dashed curves) simulated transmission spectra of the FP-based accelerometer for various accelerations.

mirror is positioned at the end of a waveguide collimator. The waveguide collimator is used to reduce the numerical aperture of the beam in the horizontal direction, reducing the divergence of the input beam. A gap of 27 μm was considered for the FP cavity to enable its future interrogation using a tunable laser with a 30-nm dynamic range. Due to the sidewall scalloping phenomenon generated by the DRIE process, the sidewall surfaces of the DBR mirrors are not very smooth. A smooth sidewall morphology is essential to minimize light scattering (which generates optical losses and reduces the quality factor of the cavity) and preserve collimated light beam when the etched sidewall is used as a mirror surface. The rms surface roughness of the DBR sidewalls was estimated to be 50 nm from the scanning electron micrograph (SEM) pictures. Adding oxygen gas during the etching reduces the roughness [17]. Applying this technique to our device diminished the sidewall roughness to 30 nm.

IV. Characterization

The same experimental setup as our previous report [18] is used to characterize the sensor (Fig. 7). Light from a broadband source (1520–1620 nm) is butt coupled to the input waveguide through an optical fiber. The transmitted light is collected by an output optical fiber butt coupled to the output tapered waveguide and sent to an optical spectrum analyzer. The whole setup is attached to an inclinable board that can be tilted. Acceleration is applied to the device as a consequence of gravity by tilting the board $(g \sin\theta)$. The transmission peak of the FP shifts to shorter wavelengths, while the angle of inclination is increased (sensing accelerations from 0.180 to 0.307 g). Fig. 8 compares the measured and simulated transmission spectra of the device.

The initial transmission peak is 1534.5 nm, while 0.18-g acceleration is applied. As acceleration is increased, the air gap between the two Bragg reflectors decreases, resulting in transmission peak shift toward shorter wavelengths. We believe that the presence of sidebands can be due to the formation of FP cavities between input/output fiber end facet and input/output waveguide end facet and misalignments (between fiber and waveguide) after tilting the setup. The filter can be tuned continuously over 30 nm. A larger tuning range could be achieved using a smaller gap since it would provide a larger free spectral range (FSR). The full-width at half-maximum of the peaks is 3 nm. A transfer matrix method is used to simulate the transmitted light across the FP filter by considering a plane wave incident beam. Due to the fabrication imperfections (generated by photolithography and etching processes), the measured peaks are not exactly located at the same locations predicted by the simulations.

V. Performance

A. Sensor Dynamic Range

Several optical resonances are available in the spectral response of FP-based sensors. The dynamic range of the device is limited to the half symmetric optical range between two adjacent resonances or FSR; therefore, from (3), the maximum dynamic range is calculated as

$$\Delta a_{\max} = \frac{m\omega_n^2}{2} \times \frac{FSR}{2}. \tag{9}$$

Knowing that the FPM resonance order for a 27-μm gap is $m = 52$, the maximum dynamic range of the sensor would be $\Delta a_{\max} = 263$ mg.

B. Sensor Sensitivity

According to (2), the sensitivity of the sensor depends on two factors: mechanical part (ω_n) which is related to the sensor architecture and optical part $(\Delta\lambda)$ which is related to the FP finesse. Fig. 9 shows the resonant wavelength shift of the FPM versus applied acceleration extracted from Fig. 8, yielding a sensitivity of 90 nm/g.

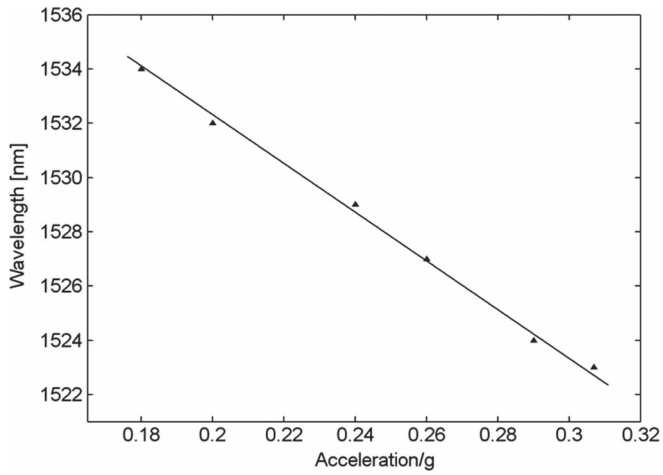

Fig. 9. Measured wavelength shift versus applied acceleration.

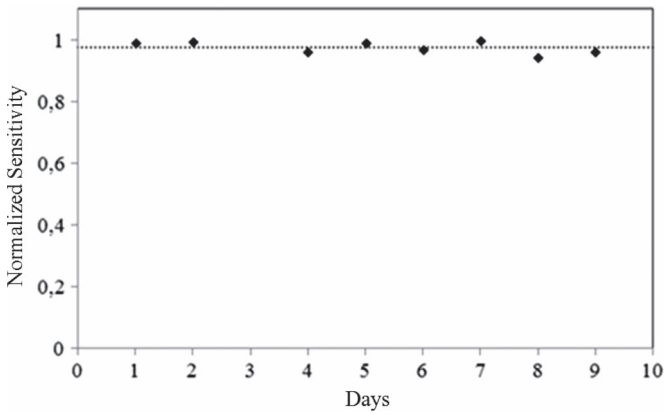

Fig. 10. Measurement of the sensitivity of the device over a nine-day period.

C. Sensor Resolution

According to (3) and considering an optical spectrum analyzer with a wavelength resolution of $\Delta\lambda = 10$ pm, assuming that we are only limited by the optical spectrum analyzer resolution, the resolution δa of our device is calculated as

$$\delta a = \frac{m\omega_n^2 \Delta\lambda}{2} = \frac{52(2\pi 409)^2 \times 10\ \text{pm}}{2} = 175\ \mu\text{g}. \quad (10)$$

From Fig. 9 and applying the same assumption, a 111-μg resolution is expected for our sensor which approximates what was calculated in (10). According to (3), better resolution and sensitivity can be achieved if the natural frequency is lowered and the order of interference is reduced by decreasing the cavity gap.

D. Sensor Stability

A stability test was performed. A piezoelectric actuator was used to apply high acceleration over a long period of time. The actuator was driven at 700 Hz, inducing an acceleration of ± 6 g on the system over a nine-day period. A measure of sensitivity similar to the one shown in Fig. 9 was taken each day while the actuator was switched off. The results are reported in Fig. 10. The measured average sensitivity is 87 nm/g.

VI. Conclusion

An integrated FP-based optical MEMS accelerometer has been presented. The device has been fabricated on a SOI substrate using one single mask. As a consequence of acceleration, the length of the FP cavity changes and modifies the FP resonance. The static response of the sensor has been studied, demonstrating 90-nm/g sensitivity, 111-μg resolution, and 263-mg dynamic range. The device has the potential to reach μg resolution. The sensor response stability has also been tested, showing high stability over time. These characteristics along with its light weight and low power consumption make the device appropriate for microsatellite navigation purposes.

Acknowledgment

The authors would like to thank J. Zou, B. Wong, R. V. Kruzelecky, and W. Jamroz from MPB Communications Inc. and P. Melanson and L. Ngo-Phong from the Canadian Space Agency for their constructive suggestions.

References

[1] O. Coumar, "Potential applications of micro and nano technologies on space transportation systems," EADS-ST, Mureaux, France, Rep. OMB 0704-0188, Jul. 13, 2005.

[2] J. A. Plaza, A. Llobera, C. Dominguez, J. Esteve, I. Salinas, J. Garcia, and J. Berganzo, "BESOI-based integrated optical silicon accelerometer," *J. Microelectromech. Syst.*, vol. 13, no. 2, pp. 355–364, Apr. 2004.

[3] A. J. Jacobs-Cook, "MEMS versus MOMS from a system point of view," *J. Micromech. Microeng.*, vol. 6, no. 1, pp. 148–156, Mar. 1996.

[4] D. Uttamchandani, D. Liang, and B. Culshaw, "A micromachined silicon accelerometer with fibre optic interrogation," in *Proc. Inst. Elect. Eng.—Colloq. Fibre Opt. Sens. Technol.*, 1992, pp. 27–33.

[5] J. Marty, A. Malki, C. Renouf, P. Lecoy, and F. Baillieu, "Fiber-optic accelerometer using silicon micromachined techniques," *Sens. Actuators A, Phys.*, vol. 46/47, no. 1–3, pp. 470–473, Mar./Apr. 1995.

[6] B. Guldimann, P. Dubois, P.-A. Clerc, and N. F. de Rooij, "Fiber optic-MEMS accelerometer with high mass displacement resolution," in *Proc. 11th Int. Conf. Solid-State Sens. Actuators*, Munich, Germany, Jun. 10–14, 2001, pp. 438–441.

[7] N. C. Loh, M. A. Schmidt, and S. R. Manalis, "Sub-10 cm^3 interferometric accelerometer with nano-g resolution," *J. Microelectromech. Syst.*, vol. 11, no. 3, pp. 182–187, Jun. 2002.

[8] N. A. Hall, M. Okandan, R. Littrell, D. K. Serkland, G. A. Keeler, K. Peterson, B. Bicen, C. T. Garcia, and F. L. Degertekin, "Micromachined accelerometers with optical interferometric read-out and integrated electrostatic actuation," *J. Microelectromech. Syst.*, vol. 17, no. 1, pp. 37–44, Feb. 2008.

[9] J. Yang, S. Jia, and Y. Dua, "Novel optical accelerometer based on Fresnel diffractive micro lens," *Sens. Actuators A, Phys.*, vol. 151, no. 2, pp. 133–140, Apr. 2009.

[10] D. Tang, D. Zhao, Y. Wang, X. Zhang, Z. Liang, and F. Guo, "A MOEMS accelerometer based on photoelastic effect," *Int. J. Light Electron Opt.*, vol. 122, no. 7, pp. 635–638, Apr. 2011.

[11] G. Schröpfer, W. Elflein, M. de Labachelerie, H. Porte, and S. Ballandras, "Lateral optical accelerometer micromachined in (100) silicon with remote readout based on coherence modulation," *Sens. Actuators A, Phys.*, vol. 68, no. 1–3, pp. 344–349, Jun. 1998.

[12] S. Baglio, M. Bloemer, M. Cappeddu, M. C. Larciprete, N. Savalli, M. Scalora, and C. Trigona, "Novel SOI inertial sensors with optical readout based on transparent metals," in *Proc. IEEE Sens.*, 2008, pp. 333–336.

[13] B. Ando, S. Baglio, and C. Trigona, "Design, fabrication, and characterization of BESOI-accelerometer based on photonic band gap effect," in *Proc. I2MTC*, May 13–16, 2012, pp. 2309–2312.

[14] J. John, I. Saha, R. Islam, J. Joseph, V. V. Lakshmipathy, K. Kanakaraju, Y. K. Jain, and T. K. Alex, "Planar silicon accelerometer with fiber-optic sensing: A system level study," in *Proc. SPIE*, 2003, vol. 5062, pp. 445–449.

[15] A. Perez and A. M. Shkel, "Design and demonstration of a bulk micromachined Fabry–Pérot μg-resolution accelerometer," *IEEE Sensors J.*, vol. 7, no. 12, pp. 1653–1662, Dec. 2007.
[16] E. J. Eklund and A. M. Shkel, "Factors affecting the performance of micromachined sensors based on Fabry–Pérot interferometry," *J. Micromech. Microeng.*, vol. 15, no. 9, pp. 1770–1776, 2005.
[17] B. Wu, A. Kumar, and S. Pamarthy, "High aspect ratio silicon etch: A review," *J. Appl. Phys.*, vol. 108, no. 5, pp. 051101-1–051101-20, Sep. 2010.
[18] K. Zandi, B. Wong, J. Zou, R. V. Kruzelecky, W. Jamroz, and Y.-A. Peter, "In-plane silicon-on-insulator optical MEMS accelerometer using waveguide Fabry–Perot microcavity with silicon/air Bragg mirrors," in *Proc. 23rd IEEE Int. Conf. Micro Electro Mech. Syst.*, Hong Kong, China, 2010, pp. 839–842.

Kazem Zandi received the B.Sc (with honors) degree in applied physics from Bu-Ali Sina University, Hamedan, Iran, in 1998, and the M.Sc degree in applied physics from the University of Tehran, Tehran, Iran, in 2001. He is currently working toward the Ph.D. degree in the Department of Engineering Physics, École Polytechnique de Montréal, Montréal, QC, Canada.

His research focuses on integrated microoptoelectromechanical inertial sensors.

Joseph André Bélanger received the B.Ing. degree in engineering physics from the École Polytechnique de Montréal, Montréal, QC, Canada, in 2012, where he is currently working toward the M.Sc. degree in applied science in the Microphotonics Laboratory (Prof. Yves-Alain Peter).

His research interests include microphotonics and optofluidic biosensing.

Yves-Alain Peter (S'93–M'03–SM'07) received the M.Sc. degree in physics and the Dr.Sc. degree in sciences from the University of Neuchâtel, Neuchâtel, Switzerland, in 1994 and 2001, respectively.

In 1995, he was a Research Associate in the Department of Medical Radiobiology, Paul Scherrer Institute, Switzerland. During 1995–2001, he was a Graduate Research Assistant with the Applied Optics Group, Institute of Microtechnology, University of Neuchâtel. From 2001 to 2003, he was a Postdoctoral Researcher with the Microphotonics Group, Stanford University, Stanford, CA. From 2003 to 2004, he was an R&D Engineer and Project Leader with the Swiss Center for Electronics and Microtechnology, Switzerland. He is currently an Associate Professor in the Department of Engineering Physics, École Polytechnique de Montréal, Montréal, QC, Canada. His research interests include microphotonics and microoptoelectromechanical systems.